Modern Physical Chemistry Research (2023)
Clausius Scientific Press, Canada

DOI: 10.23977/mpcr.2023.030102
ISSN 2616-1702 Vol. 3 Num. 1

Micro Structure and Magnetic Behavior of $La_{0.7}Pb_{0.3}Mn_{1-x}Co_xO_3$ Perovskite Nanomaterials

Jin Hao[1,2,#], Fengwu Du[2,#], Qing Lin[1,2,#], Pan Dong[2,*], Yun He[2], Fang Yang[1,*]

[1]*College of Biomedical Information and Engineering, Hainan Medical University, Haikou, 571199, China*
[2]*College of Physics and Technology, Guangxi Normal University, Guilin, 541004, China*
[#]*These authors contributed equally to this work.*
[*]*Corresponding author*

Keywords: perovskite materials, $LaMnO_3$, Sol-gel, structure, magnetic

Abstract: A perovskite solar cell is a solar cell using a perovskite type organic metal halide semiconductor as a light absorbing material.The perovskite solar cell precursors $La_{0.7}Pb_{0.3}Mn_{1-x}Co_xO_3$ was successfully prepared by the Sol-gel method. The experimental conditions were calcined at 950℃ for 10 hours. TG-DSC shows that the chemical reaction led to a slow endothermic process, when the temperature was above 300℃, and the formation of the lattice. The X-ray diffraction results confirmed all samples are perovskite rhombohedron (R-3C) structure, and no impurity is generated, the average grain size of the sample are 38.0nm to101.4nm. The SEM results show that the particle boundary is clear and there is little agglomeration between particles, the particle size increases and the agglomeration becomes serious with the increase of Co doping content. The FT-IR images show that the absorption peak in the low-frequency wavenumber phase of the main band at around 439 cm^{-1} and 608 cm^{-1}. The ferromagnetism of samples $La_{0.7}Pb_{0.3}Mn_{1-x}Co_xO_3$ (x=0~1.0) gradually weakens with the increase of Co doping ratio, the specific saturation magnetization of the samples reduced from 47.69 emu/g to 0.62 emu/g, while the coercivity increased from 36.79 Oe to 96.68 Oe.

1. Introduction

Manganese-based perovskite materials have attracted extensive attention of researchers, due to the giant magnetoresistance effect, magnetocaloric effect, catalytic oxidation, electrical conductivity and other outstanding features[1-2]. Perovskite type solar cells are solar cells using perovskite type organic metal halide semiconductors as light absorbing materials, belonging to the third generation of solar cells, also known as new concept solar cells[3-4]. Perovskite solar cells use organic-inorganic hybrid metal halides with perovskite crystal structure as the light absorption layer. Since 2009, they have attracted much attention due to their simple preparation method, low production cost and excellent photoelectric performance. The photoelectric conversion efficiency has rapidly increased from 3.8% to 23.7%, becoming the fastest developing photovoltaic technology at present and the most attractive emerging photovoltaic technology in the world.The industry expects that the perovskite technology can greatly reduce the manufacturing cost of photovoltaic modules while further improving the

photoelectric conversion efficiency.

In recent years, in order to further expand the application scope of manganese-based perovskite materials in practice, more and more researches have been developed towards multi-component[3-4]. Among many candidate materials, transition metal (Fe, Co, Cr, Ni) ions have similar ionic radii to B-site manganese ions, and the average ionic radius of B-site can be kept small by doping transition metal ions by breaking the valence ratio of Mn^{3+} and Mn^{4+} at the B site, the double exchange between Mn^{3+} and Mn^{4+} is weakened, and the octahedral structure of MnO_6 is distorted, resulting in a series of new physical and chemical properties[5-7]. The study of B-site co-doping of perovskite composite oxide $La_{0.7}Pb_{0.3}MnO_3$ is of great significance for understanding the internal mechanism of the material and developing new functional materials.

In recent years, many scientific researchers have made important research on the B site co-doping of perovskite composite oxide $La_{0.7}Pb_{0.3}MnO_3$. In 2007, Zhao[4] et al. studied the structure, magnetic and magnetocaloric properties of perovskite manganate $La_{1-x}Pb_xMn_{1-y-z}Cu_yO_3$, found to generate a large magnetic entropy changed near the Curie temperature T_C, employing double-exchange interactions as well as competing effects between lattice distortions induced by Cu doping, explained The maximum magnetic entropy change of the sample with Cu doping ratio of 0.01 is obtained. In 2010, Dhahri N [5-7] et al. prepared $La_{0.67}Pb_{0.33}Mn_{1-x}Co_xO_3$ ($0\leq x\leq 0.3$) material by sol-gel method and studied its structural and magnetic changes, and found that all the samples are all rhombohedral structures. With the increase of Co doping ratio, the Curie temperature decreases and the magnetic entropy change increases. When x=0.3, the maximum magnetic entropy change is 3.22 J/ (K ·kg). Tokarz W [8-9] et al. used first-principles density functional theory to study the band structures and photoemission states of $La_{2/3}Pb_{1/3}MnO_3$ and $La_{0.67}Pb_{0.33}Mn_{1-x}Fe_xO_3$. From the reports in the literature, it can be found that the doping of different elements and different preparation methods and process conditions have a great influence on the structure, morphology and magnetic properties of the synthesized samples.

Therefore, in order to further improve the morphology of the sample and expand the application range of the perovskite composite oxide $La_{0.7}Pb_{0.3}MnO_3$, according to the synthesis process of the sample explored, the Co ion pair $La_{0.7}Pb_{0.3}MnO_3$ manganese with a similar magnetic moment to the Mn ion was selected. The B site of the oxide is co-doped. Under this synthesis method, the change law of the microstructure and magnetic properties of perovskite solar cell precursors $La_{0.7}Pb_{0.3}Mn_{1-x}Co_xO_3$ is mainly studied, and the ionic radius effect produced by the doping of transition metal Co and perovskite is revealed. Intrinsic link between microstructure and magnetic properties of manganese oxide materials. Lay the theoretical and experimental foundation for the development and application of new functional materials.

2. Experimental

2.1. Material Preparation

In this experiment, $La_{0.7}Pb_{0.3}Mn_{1-x}Co_xO_3$ doped with different proportions of Co was compared and studied. The specific steps are as follows:

According to the molar ratio of $La_{0.7}Pb_{0.3}Mn_{1-x}Co_xO_3$, weigh the total amount of substances as 0.01mol La $(NO_3)_3$, Pb $(NO_3)_2$, and 0.01mol of Mn $(NO_3)_2$(50%) solution, Co $(NO_3)_2 \cdot 6H_2O$;

According to the mol ratio of the complexing agent and the metal ion being 1:1, take by weighing 11 parts of citric acid monohydrate whose amount is 0.02mol;

The weighed nitrates and complexes were dissolved and mixed with deionized water, respectively, to obtain a precursor solution. Label the 11 solutions as N_1~N_{11};

The precursor solution was stirred in a water bath at 50℃, the pH of the solution was adjusted to

about 7 with ammonia water, a small amount of ethylene glycol was added dropwise as a dispersant, and the stirring and evaporation were continued until the solution was evaporated to dryness to obtain a wet gel;

The wet gel was placed in a digital display drying box and dried at 100℃ for 24h to obtain a dry gel;

Use alcohol self-propagating combustion to obtain black precursor powder;

After fully grinding the precursor powder, put it into a muffle furnace, control the heating rate to be 2.5℃ per minute, and calcinate at 950℃ for 10 hours to obtain a black shiny sample powder.

2.2. Characterization Method

In this paper, the X-ray diffractometer (D/max-2500v/pc) of Rigaku Company in Japan was used to characterize and analyze the phase structure of the sample; the FT-IR spectrometer of Perkin Elmer Company was used to analyze the possible functional groups and internal chemical bonds in the sample; The EVO18 electron scanning microscope of ZEISS company was used to test the microscopic morphology of the sample; The VSM-100 vibrating sample magnetometer of Yingpu Magnetics was used to test the hysteresis loop of the sample at room temperature.

3. Results and discussion

3.1. DTG-DSC Analysis

In order to study the thermal decomposition process and quality change of the xerogel precursor at high temperature, TG-DSC test was carried out on the xerogel precursor of $La_{0.7}Pb_{0.3}Mn_{0.9}Co_{0.1}O_3$. Figure 1 shows TG-DSC test results of the $La_{0.7}Pb_{0.3}Mn_{0.9}Co_{0.1}O_3$ under N_2 atmosphere.

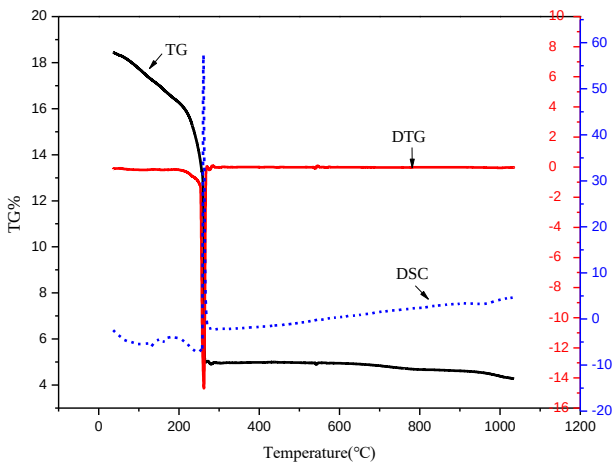

Figure 1: TG-DTG diagram of $La_{0.7}Pb_{0.3}Mn_{0.9}Co_{0.1}O_3$

It can be seen from the TG curve that the weight loss ratio of the xerogel is 3.85% at 0~100℃, and there is a corresponding endothermic peak in the DSC curve, which is mainly caused by the loss of water in the precursor; at 100℃ The weight loss ratio at 100~200℃ is 7.97%, and there are two small absorption peaks in the DSC curve, which are mainly caused by the gradual decomposition of crystal water and organic matter in the precursor[9-10]; There is a large weight loss of about 49.21% near 262℃, and there is an obvious endothermic peak and exothermic peak in the DSC curve, which is attributed to the strong oxidation reaction of citric acid or the violent decomposition of different metal nitrates. The hydrocarbon components in the precursor almost completely disappeared, resulting in

significant weight loss [10]; when the temperature was above 300℃, the chemical reaction led to a slow endothermic process, and the mass of the precursor remained basically unchanged, and finally The composite material is about 26.56% of the total mass of the precursor, corresponding to the formation of the lattice.

3.2. Structural Analysis

Figure 2 is the XRD pattern of the sample $La_{0.7}Pb_{0.3}Mn_{1-x}Co_xO_3$ (x=0~1.0), the crystal structure of all samples is perovskite rhombohedron (R-3C) structure, and no impurity is generated. It shows that the single phase of the sample is good and the synthesis quality is high. Its lattice parameters are in perfect agreement with the standard card (JCPDS: 70-3942) values.

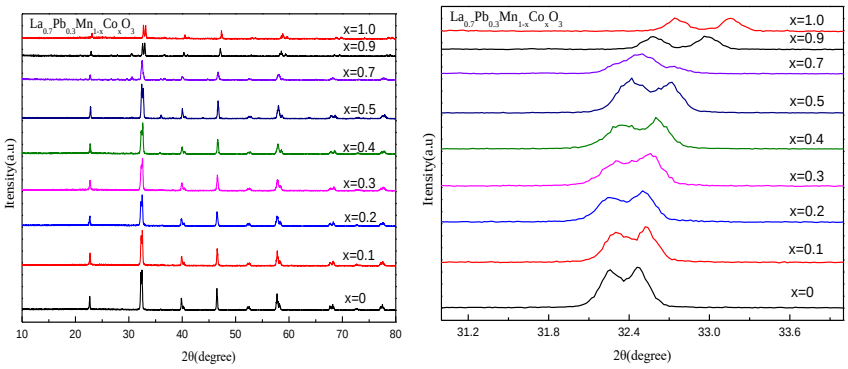

Figure 2: XRD pattern of sample $La_{0.7}Pb_{0.3}Mn_{1-x}Co_xO_3$

And as the doping ratio of Co increases, the main diffraction peak shifts to a high angle; the lattice parameters under different doping ratios can be obtained by JADE fitting as shown in Table 1.

$$2d\sin\theta=n\lambda \tag{1}$$

According to the Bragg equation (1), λ is constant, if θ is larger then d is smaller, and the unit cell parameter become smaller. From the enlarged image of the main diffraction peak in Fig.2, it can be seen that the position of the main diffraction peak increases with the increase of the Co doping ratio. The angle is shifted, and the corresponding lattice parameter decreases. Figure 3 shows the relationship between the unit cell parameterand and the Co doping amount x for the sample $La_{0.7}Pb_{0.3}Mn_{1-x}Co_xO_3$. The figure shows that the lattice constant and the unit cell volume.

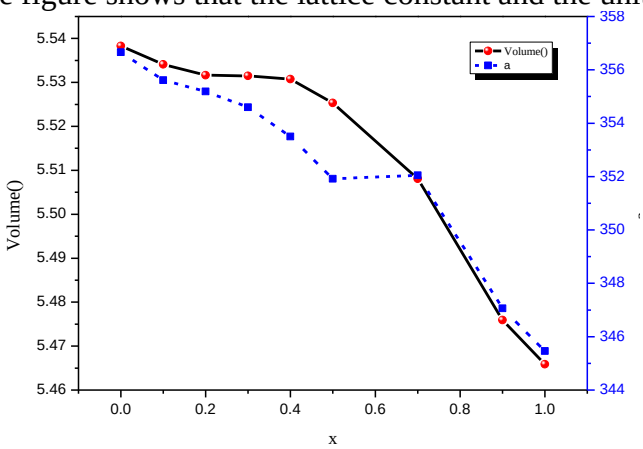

Figure 3: Variation trend of unit cell parameters of sample $La_{0.7}Pb_{0.3}Mn_{1-x}Co_xO_3$ with Co doping content x

Table 1: The unit cell parameters of $La_{0.7}Pb_{0.3}Mn_{1-x}Co_xO_3$

parameter	x=0	x=0.1	x=0.2	x=0.3	x=0.4
Space groups	R-3c(167)(hexagonal)	R-3c(167)(hexagonal)	R-3c(167)(hexagonal)	R-3c(167)(hexagonal)	R-3c(167)(hexagonal)
a(Å)	5.53829	5.53412	5.53166	5.53149	5.53075
b(Å)	5.53829	5.53412	5.53166	5.53149	5.53075
c(Å)	13.42685	13.40746	13.40335	13.38219	13.34430
Vol($Å^3$)	356.66	355.61	355.19	354.6	353.5
Crystallite Size(Å)	810(17)	604(14)	543(14)	414(8)	476(9)
θ1	32.242	32.262	32.217	32.258	32.316
θ2	32.470	32.533	32.508	32.571	32.609
△2θ	0.228	0.271	0.291	0.313	0.293
parameter	x=0.5	x=0.7	x=0.9	x=1.0	
Space groups	R-3c(167)(hexagonal)	R-3c(167)(hexagonal)	R-3c(167)(hexagonal)	R-3c(167)(hexagonal)	
a(Å)	5.52534	5.50809	5.47592	5.46588	
b(Å)	5.52534	5.50809	5.47592	5.46588	
c(Å)	13.31043	13.39886	13.36474	13.35213	
Vol($Å^3$)	351.92	352.05	347.06	345.46	
Crystallite Size(Å)	609(10)	380(9)	734(18)	906(27)	
θ1	32.366	32.458	32.573	32.747	
θ2	32.714	32.731	32.976	33.159	
△2θ	0.348	0.273	0.403	0.412	

The decreasing trend may be related to the lattice distortion caused by Co atoms replacing Mn atoms into the $LaMnO_3$ lattice. Through the change of Δ2θ, it is found that with the increase of Co doping amount x, Δ2θ also increases, indicating that the doping of Co does indeed cause the change of the lattice.Furthermore, using the Scherrer formula:

$$D=0.94\lambda/\beta\cos\theta \tag{2}$$

The average grain size of the sample can be calculated, where β is the full width at half maximum of the main diffraction peak, λ is the x-ray wavelength, and θ is the diffraction angle. The calculated average grain sizes of the crystals are 81.0 nm, 60.4 nm, 54.3 nm, 41.4nm, 47.6nm, 60.9nm, 38.0nm, 73.4nm, 101.4nm, the samples are all nanomaterials.

Figure 4 shows the SEM images of $La_{0.7}Pb_{0.3}Mn_{1-x}Co_xO_3$ (x=0, 0.1, 0.5, 0.9) nanoparticles. It can be seen from the figure 4 that when the doping ratio is 0 and 0.1, the particle boundary of $La_{0.7}Pb_{0.3}Mn_{0.9}Co_{0.1}O_3$ manganese oxide is clear, the morphology is neat, and the average particle size is relatively uniform, and there is little agglomeration between particles; with the increase of Co doping ratio, the particle size of the sample increases, when$x$= 0.5, some particles agglomerate; when x= 0.9, the agglomeration is the most serious, and the particle size increases, this may be due to the mismatch between adjacent layers caused by the increase of the Co doping ratio, which is easy to distort the lattice. In addition, with the increase of the Co substitution amount x, the perovskite structure will generate oxygen vacancies, which may also lead to changes in the unit cell structure and increase agglomeration, the macroscopic appearance of particle shape becomes irregular, and the particle size is inconsistent.

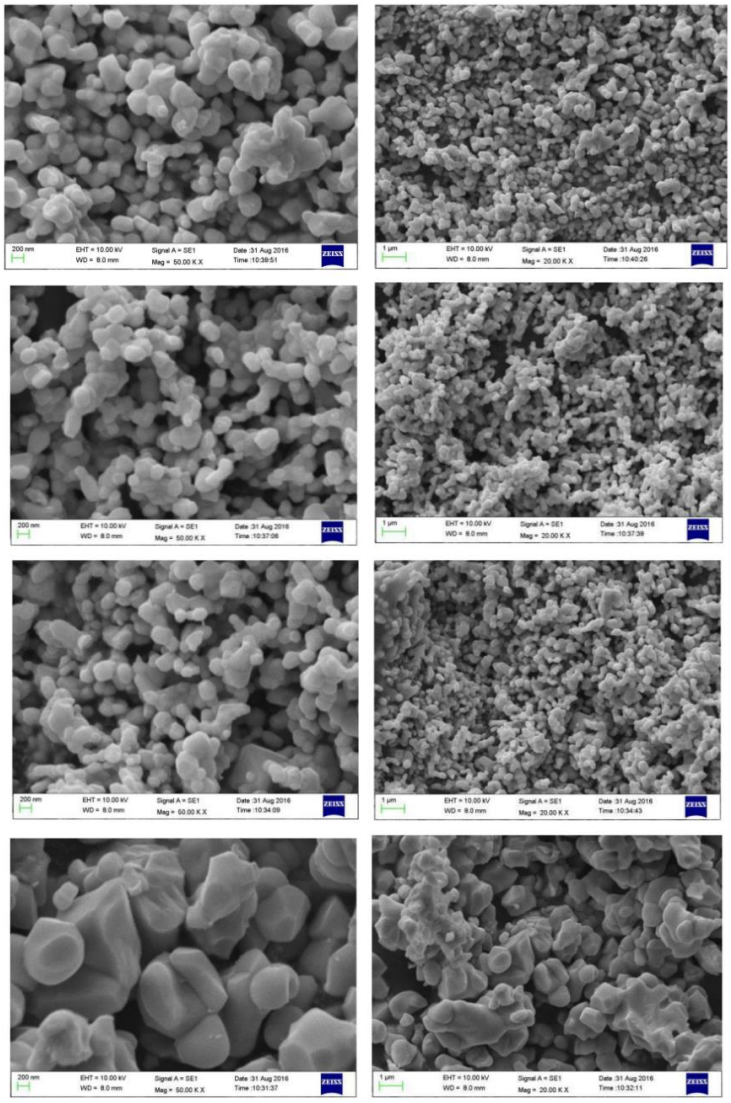

Figure 4: SEM image of sample $La_{0.7}Pb_{0.3}Mn_{1-x}Co_xO_3$ (x=0, 0.1, 0.5, 0.9)

The FT-IR image of the sample $La_{0.7}Pb_{0.3}Mn_{1-x}Co_xO_3$ (x=0.1~0.9) is shown in Figure 5, and the diagram shows that all samples appear obvious infrared absorption peak at around 439 cm^{-1}, 608 cm^{-1}, 1630 cm^{-1}, 3432 cm^{-1}. The illustration shows the absorption peak in the low-frequency wavenumber phase of the main band at around 439 cm^{-1} and 608cm^{-1}, which can be attributed to the bending vibration of O-Mn-O caused by the Jahn-teller distortion and the stretching vibration of Mn-O in the MnO_6 regular octahedron. The changes of Mn-O bond length and O-Mn-O bond angle are all related to the conditions of Mn-O stretching vibration and O-Mn-O bending vibration [11]. The vibrational absorption peak of the Co-doped sample is strengthened at around 608 cm^{-1}, which indicates that the MnO_6 octahedral distortion is partly caused by the Co doping. The symmetric stretching vibration of the carboxyl radical is found around the wavenumber of 2350 cm^{-1} [3], there is a broad peak at about 3431 cm^{-1} corresponding to the O-H stretching vibration of water molecules. And there is a strong stretch vibration at 1630 cm^{-1}, it is attributed to the bending vibrations of the surface water molecules H-O-H [12].

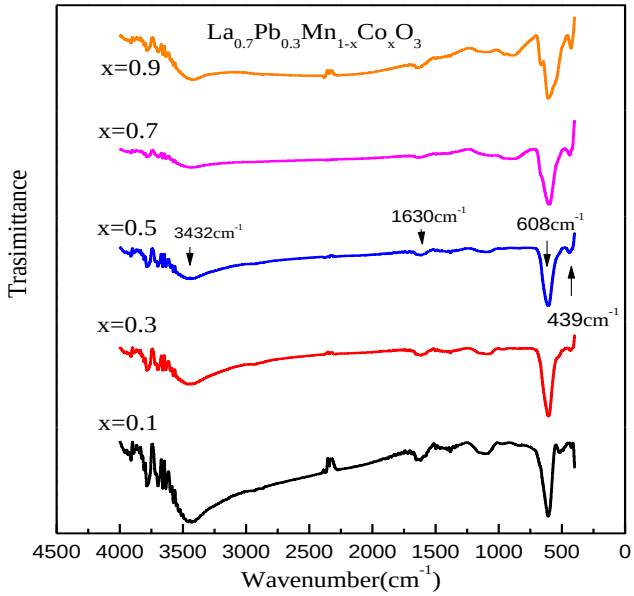

Figure 5: FT-IR image of sample $La_{0.7}Pb_{0.3}Mn_{1-x}Co_xO_3$ (x=0.1~0.9)

3.3. Magnetic Performance Analysis

The hysteresis loops of the sample $La_{0.7}Pb_{0.3}Mn_{1-x}Co_xO_3$ nanomaterials at room temperature are shown in Figure 6. The hysteresis loops of all samples are closed curves, and the samples $La_{0.7}Pb_{0.3}MnO_3$ showed obvious ferromagnetic at room temperature , the magnetization basically reaches saturation around 0.2T, and it is a soft magnetic material with small coercivity.

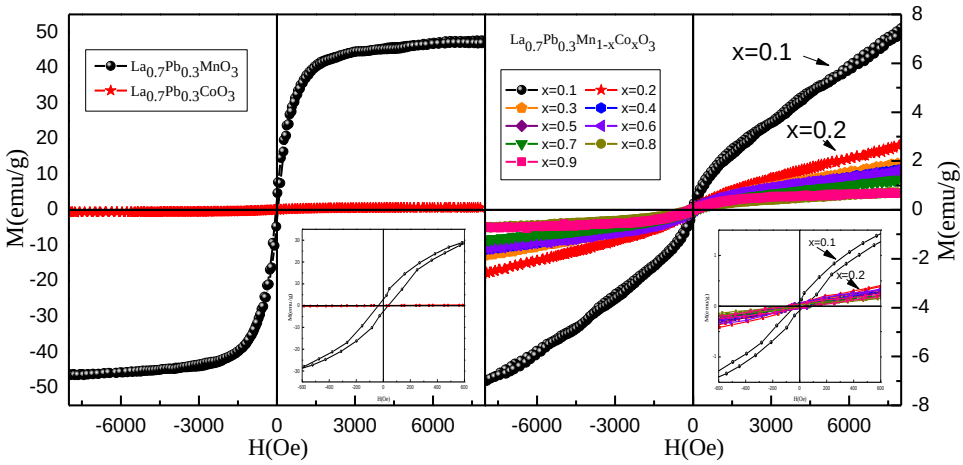

Figure 6: Magnetic hysteresis loop of sample $La_{0.7}Pb_{0.3}Mn_{1-x}Co_xO_3$

Table 2 shows the specific magnetic parameters of the $La_{0.7}Pb_{0.3}Mn_{1-x}Co_xO_3$ polycrystalline material. It can be seen from the table 2 that the specific saturation magnetization of the samples are 47.69 emu/g, 7.46 emu/g, 2.65 emu/g, 1.90 emu/g, 1.64 emu/g, 1.46 emu/g, 1.60 emu/g, 1.24 emu/g, 0.72 emu/g, 0.72 emu/g, 0.62 emu/g, respectively. The ferromagnetism of the sample $La_{0.7}Pb_{0.3}Mn_{1-x}Co_xO_3$ varies with the increase of Co doping amount showed a decreasing trend. In order to more clearly reflect the changing law of magnetic parameters with the Co doping amount x, the relationship between the specific saturation magnetization, coercivity, remanent magnetization and doping amountxas shown in Figure 7.

Table 2: Magnetic parameters of sample $La_{0.7}Pb_{0.3}Mn_{1-x}Co_xO_3$ after calcination at 950°C for 10 hours

x	M_S(emu/g)	M_r(emu/g)	M_r/ M_S	H_C(Oe)	Loop area
x=0	47.69	2.85	0.060	36.79	0.8
x=0.1	7.46	0.10	0.013	34.17	0.2
x=0.2	2.65	0.06	0.023	68.32	0
x=0.3	1.90	0.04	0.022	65.46	0
x=0.4	1.64	0.04	0.026	44.32	0
x=0.5	1.46	0.06	0.041	96.68	0
x=0.6	1.60	0.06	0.038	80.96	0
x=0.7	1.24	0.04	0.030	75.14	0
x=0.8	0.72	0.03	0.041	66.73	0
x=0.9	0.72	0.04	0.062	77.68	0
x=1.0	0.62	0.05	0.085	89.38	0

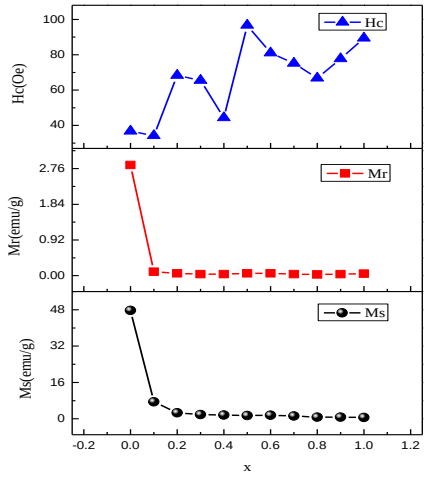

Figure 7: Variation trend of magnetic parameters of sample $La_{0.7}Pb_{0.3}Mn_{1-x}Co_xO_3$ with Co doping content.

The diagram shows that the specific saturation magnetization and remanent magnetization decrease rapidly with the increase of Co doping ratio, while the coercivity increases with the increase of Co doping ratio; when the doping ratio is x=0.1, the magnetization strength is still not saturated at 0.8T, and it is weak ferromagnetic. When the doping ratio is further increased, the ferromagnetism of the nanoparticle material basically disappears, which may be due to the fact that Co doping weakens the double exchange between Mn^{4+} and Mn^{3+} ions, resulting in the decrease in the mobility of the e_g electrons of Mn^{3+}, which makes the ferromagnetism is weakened. In addition, when Co is doped on the Mn site, because the ionic radii of Co and Mn^{3+} are close, the substitution of Co on the Mn site will not change the bond length and bond angle of the Mn-O bond, so the lattice effect can be completely eliminated [13-14].

4. Conclusion

The perovskite solar cell precursors $La_{0.7}Pb_{0.3}Mn_{1-x}Co_xO_3$ was successfully prepared by the Sol-gel method.The XRD results show that the lattice constant and the unit cell volume both show a decreasing trend with the increase of Co doping ratio. The Mn-O stretching vibration and O-Mn-O bending vibration peaks of the sample $La_{0.7}Pb_{0.3}Mn_{1-x}Co_xO_3$ were found at the low-frequency wavenumber stage of 608 cm^{-1} and 439 cm^{-1}, and the vibration absorption peak around 608 cm^{-1} of

the sample is strengthened after Co doping, indicating that the MnO_6 octahedral distortion is partly caused by the doping of Co^{3+}.The SEM results show that the particle boundary is clear, the morphology is neat, and the average particle size is relatively uniform, and there is little agglomeration between particles for the sample $La_{0.7}Pb_{0.3}Mn_{0.9}Co_{0.1}O_3$.According to the particle size statistics, the average particle size of the sample $La_{0.7}Pb_{0.3}Mn_{1-x}Co_xO_3$ (x=0.1, 0.5, 0.9) is 202.59 nm, 246.11 nm, 264.62 nm respectively, indicating that the samples obtained in our experiment are many crystal material.The VSM results show that the ferromagnetism of samples $La_{0.7}Pb_{0.3}Mn_{1-x}Co_xO_3$($x$=0~1.0) gradually weakens with the increase of Co doping ratio. With the increase of Co content, the specific saturation magnetization and remanent magnetization decrease rapidly, while the coercivity increases; when the doping ratio is x=0.1, the magnetization is not saturated at 0.8T, which is weak ferromagnetism; when the doping ratio is further increased, the ferromagnetism of nanoparticle materials basically disappears.

Acknowledgment

This work was financially supported by the National Natural Science Foundation of China (NO.11364004). J.Hao and F.Du contributed equally to this work. All authors discussed the results and commented on the manuscript.F.Yang and P.Dang are co-corresponding authors contributed equally.

References

[1] P Kulandaivelu, K Sakthipandi, P SenthilKumar, V Rajendran, Mechanical properties of bulk and nanostructured $La_{0.61}Sr_{0.39}MnO_3$ perovskite manganite materials. Journal of Physics and Chemistry of Solids, 2013, 74: 205-214.

[2] K Sakthipandi, V Rajendran. On-line phase transitions of bulk and nanocrystalline $La_{1-x}Pb_xMnO_3$ (x=0.3, 0.4, and 0.5) perovskite manganite materials using ultrasonic measurements. Materials Chemistry and Physics, 2013, 138: 581-592.

[3] S Thirumalairajan, K Girija, I Ganesh, D Mangalaraj, C Viswanathan, A Balamurugan, N Ponpandian. Controlled synthesis of perovskite $LaFeO_3$ microsphere composed of nanoparticles via self-assembly process and their associated photocatalytic activity. Chemical Engineering Journal, 2012, 209:420-428.

[4] B. C. Zhao; Y. P. Sun; X. B. Zhu; W. H. Song. Magnetic and magnetocaloric properties of Cu-substituted $La_{1-x}Pb_xMnO_3$ (x=0.14) single crystals. Journal of Applied Physics, 2007, 101(5): 053920.

[5] Dhahri N, Dhahri A, Cherif K, et al. Effect of Co substitution on magnetocaloric effect in $La_{0.67}Pb_{0.33}Mn_{1-x}Co_xO_3$ ($0.15 \le x \le 0.3$). Journal of Alloys and Compounds, 2010, 507(2): 405-409.

[6] Hyodo T, Hayashi M, Miura N, et al. Catalytic Activities of Rare-Earth Manganites for Cathodic Reduction of Oxygen in Alkaline Solution. Journal of The Electrochemical Society, 1996, 143(11): L266-L267.

[7] Nakamura T, Misono M, Yoneda Y. Catalytic Properties of Perovskite-type Mixed Oxides, $La_{1-x}Sr_xCoO_3$. Bulletin of the Chemical Society of Japan, 1982, 55(2): 394-399.

[8] Miyoshi S, Hong J O, Yashiro K, et al. Lattice expansion upon reduction of perovskite-type $LaMnO_3$ with oxygen-deficit nonstoichiometry. Solid State Ionics, 2003, 161(3): 209-217.

[9] Heel A, Holtappels P, Graule T, et al. On the synthesis and performance of flame-made nanoscale $La_{0.6}Sr_{0.4}C_OO_{3-\delta}$ and its influence on the application as an intermediate temperature solid oxide fuel cell cathode. Journal of Power Sources, 2010, 195(19): 6709-6718.

[10] Esquirol A, Brandon N P, Kilner J A, et al. Electrochemical Characterization of $La_{0.6}Sr_{0.4}Co_{0.2}Fe_{0.8}O_3$ Cathodes for Intermediate-Temperature SOFCS. Journal of The Electrochemical Society, 2004, 151(11): A1847-A1855.

[11] Adler S B Factors governing oxygen reduction in solid oxide fuel cell cathodes. Chemical reviews, 2004, 104(10): 4791-4844.

[12] Zener C. Interaction between the d-shells in the transition metals. II. Ferromagnetic compounds of manganese with perovskite structure. Physical Review, 1951, 82(3): 403.

[13] Dhahri N, Dhahri A, Cherif K, et al. Effect of Co substitution on magnetocaloric effect in $La_{0.67}Pb_{0.33}Mn_{1-x}Co_xO_3$ ($0.15 \le x \le 0.3$). Journal of Alloys and Compounds, 2010, 507(2): 405-409.

[14] Tokarz W, Kowalik M, Zalecki R, et al. Electronic band structure and photoemission states of $La_{0.67}Pb_{0.33}Mn_{1-x}Fe_xO_3$. Radiation Physics and Chemistry, 2013, 93: 37-39.